#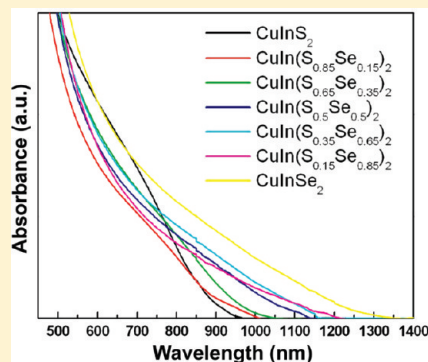 Quaternary CuIn(S$_{1-x}$Se$_x$)$_2$ Nanocrystals: Facile Heating-Up Synthesis, Band Gap Tuning, and Gram-Scale Production

Ming-Yi Chiang,[†] Shu-Hao Chang,[†] Chia-Yu Chen, Fang-Wei Yuan, and Hsing-Yu Tuan*

Department of Chemical Engineering, National Tsing Hua University, Hsinchu, Taiwan 30013, Republic of China

S *Supporting Information*

ABSTRACT: Tetragonal chalcopyrite CuIn(S$_{1-x}$Se$_x$)$_2$ ($0 \leq x \leq 1$) nanocrystals were synthesized by reacting a mixture of CuCl, InCl$_3$, S, and Se in the presence of oleylamine at 265 °C. The S/Se composition ratio in the CuIn(S$_{1-x}$Se$_x$)$_2$ could be tuned across the entire composition range of *x* from 0 to 1 by modulating the S/Se reactant mole ratio. The tetragonal lattice constants, that is, *a* and *c*, increase linearly with the increase of Se content, following Vegard's law. The band gap energies of CuIn(S$_{1-x}$Se$_x$)$_2$ nanocrystals could be tuned in the range between 0.98 and 1.46 eV and 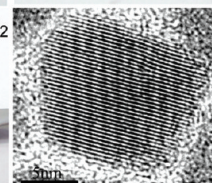change nonlinearly with respect to *x*, deriving a bowing parameter of 0.17 eV. In addition, the method developed in this study was scalable to achieve gram-scale production of stoichiometry-controlled CuIn(S$_{1-x}$Se$_x$)$_2$ and CuIn$_{1-x}$Ga$_x$Se$_2$ nanocrystals.

■ INTRODUCTION

CuIn(Se,S)$_2$ (i.e., CIS) compound materials have been well-known as promising light-absorbing materials for thin film solar cells because they are direct band gap materials with intrinsic high optical absorbing coefficients and desired optical energy gap energies (CuInSe$_2$, 1.0 eV; CuInS$_2$, 1.5 eV).[1−5] CIS-based solar cells demonstrate solar energy conversion efficiency of ∼14%,[4,5] higher than other thin film solar cells such as a-Si based photovoltaic devices. However, manufacturing processes for CIS-based solar cells mainly rely on high-cost and complicated vacuum-based tools, yielding expensive module prices and increasing their commercialization difficulty. Recently, there have been increasing efforts in developing nonvacuum, solution-based methods to fabricate solar cells via cost-effective, roll-to-roll, and high-throughput procedures.[6] CIS nanocrystals are promising precursors for absorber deposition because these stoichiometric nanocrystals may not only reduce film composition heterogeneity over large device areas, but also alleviate film cracking problems during postselenization annealing.[7] High-quality, narrow-sized CIS nanocrystals could be synthesized by arrested precipitation routes.[8−17] CIS nanocrystals exhibit superior dispersibility in a wide range of solvents and could be used as nanocrystal inks for absorbing layer deposition via various wet processing methods such as spin-coating, dip-coating, inject-printing, and spray-deposition. Several examples regarding incorporating CIS nanocrystals into solar cell fabrications have been recently reported.[8,14−16] For example, Guo et al. made a CIS absorber layer by drop-casting nanocrytals onto a Mo-coated soda lime glass followed by traditional selenization annealing, and the fabricated device exhibited solar energy conversion efficiencies as high as

4.17%.[15,16] Panthani et al. showed CuInSe$_2$ nanocrystal solar cells exhibiting efficiency of 0.24% without any postannealing procedures.[14] Li et al. reported CuInSe$_2$ nanocrystal solar cells in which the absorber was made by in situ formation of CuInS$_2$ nanocrystal film, and the devices yielded conversion efficiency up to 4.0%.[8]

The band gap energies of CuIn(S$_{1-x}$Se$_x$)$_2$ solid solution (∼1−1.5 eV) are in the range of optimum band gap energies for single junction solar cells.[18−22] Motivated by this advantageous characteristic, studies on band gap tuning of quaternary-alloyed CuIn(S$_{1-x}$Se$_x$)$_2$ have been investigated by a number of different methods, including horizontal Bridgman,[23] chemical spray pyrolysis,[24] S or Se thermal diffusion,[25] microwave irradiation,[21,22] r.f. sputtering,[26] melt and annealing,[19] and solution methods.[27−29] For semiconductor nanocrystals, although the quantum confinement effect can tune the band gap fall in the optimized absorption region,[30] this effect generally vanishes while nanocrystals form a dense film or sinter into a polycrystalline layer. Therefore, composition-mediated band gap tuning is a more robust approach to keep the absorber optical property.[31] However, stoichiometric control of quaternary nanocrystals is much more challenging as compared to that of ternary nanocrystals[32−38] because reactions easily suffer from unwanted side-reactions and usually yield products containing a plurality of compositional phases due to their high degree of phase complexity. Recent studies have shown that band gap engineering of quaternary nanocrystals

such as $CuIn_{1-x}Ga_xSe_2$,[14,39] $CuGa_xIn_{2-x}S_{3.5}$,[40] $CuIn_xTl_{2-x}S_{3.5}$,[40] $CuIn_{1-x}Ga_xS_2$,[41] $ZnS-AgInS_2$,[42] $(CuInS_2)_x(ZnS)_{1-x}$[43] Zn_x-$Cd_{1-x}S_ySe_{1-y}$,[44] and $(Cu_2Sn)_{x/3}Zn_{1-x}S$[45] could be achieved by colloid routes.

Here, we report the high-yield synthesis of chalcopyrite $CuIn(S_{1-x}Se_x)_2$ nanoparticles with controllable S/Se ratio using a facile heating-up method. A mixture of CuCl, InCl$_3$, S, Se, and oleylamine was gradually heated to 265 °C, and the reactions were held at that temperature for hours to enable quaternary $CuIn(S_{1-x}Se_x)_2$ formation. By varying the S/Se reactant molar ratio, the S/Se ratio in the $CuIn(S_{1-x}Se_x)_2$ nanocrystals could be controlled, and the band gap energies of $CuIn(S_{1-x}Se_x)_2$ could be tuned in the range between 0.98 and 1.46 eV, sitting between the band gaps of bulk CuInSe$_2$ and CuInS$_2$. Furthermore, considering a large number of CIS or $CuIn_{1-x}Ga_xSe_2$ (CIGS) nanocrystals might be in need of supply for nonvacuum absorber deposition processes, a general mass-production method is highly requested. We demonstrate that the method developed here could be readily scaled for gram-scale production of stoichiometry-controlled $CuIn(S_{1-x}Se_x)_2$ and $CuIn_{1-x}Ga_xSe_2$ nanocrystals.

■ EXPERIMENTAL METHODS

Chemicals. All chemicals were used as received from the Aldrich Chemical Co., including copper(I) chloride (CuCl, 99.995+%), indium(III) chloride (InCl$_3$ anhydrous, 99.99%), gallium(III) chloride (GaCl$_3$, 99.9999%), elemental S (99.98%), elemental Se (99.99%), hexane, toluene, oleylamine (70%), and ethanol (ACS reagent grade, >99.5%).

Nanocrystal Synthesis. Precise weighing of reactants is required for the synthesis of stoichiometry-controlled $CuIn(S_{1-x}Se_x)_2$ nanocrystals. In a reaction of $CuIn(S_{1-x}Se_x)_2$ nanocrystals, 12 mL of oleylamine, 0.5 mmol of CuCl (0.049 g), 0.5 mmol of InCl$_3$(0.111 g), and 1 mmol total of elemental Se (0.000–0.079 g) and elemental S (0.000–0.032 g) were added to a 50 mL three-neck flask placed on a heating mantle. One neck with an attached condenser and stopcock valve was connected to a Schlenk line; the other neck was connected to a thermocouple for temperature monitoring and accurate temperature control; the third neck was sealed by a rubber septum. The flask was purged of oxygen and water by argon bubbling at 130 °C for 1 h with stirring. Next, the temperature of the mixture was slowly raised to 265 °C with a ramping rate of 2.3 °C/min. The reaction was held at 265 °C for 1.5 h with continuous vigorous stirring. The flask was cooled to ambient temperature by a cold water bath. The nanocrystals were isolated by precipitation with addition of 10 mL of hexane and 15 mL of ethanol followed by centrifugation at 8000 rpm for 10 min. After a washing step, the nanocrystals were in the precipitate, whereas the supernatant containing unreacted precursors and byproducts was discarded. The isolated nanocrystals were dispersed in hexane or toluene for further characterization. The typical yield of nanocrystals after washing was ~80%.

Gram-Scale Production of CuInSSe, CuIn(S$_{0.65}$Se$_{0.35}$)$_2$, and CuIn$_{0.5}$Ga$_{0.5}$Se$_2$ Nanocrystals. For gram-scale production of CuInSSe nanocrystals, the synthesis was carried out by heating a 500 mL flask containing a mixture of 120 mL of oleylamine, 0.495 g of CuCl, 1.106 g of InCl$_3$, 0.394 g of Se, and 0.161 g of S to 265 °C with a ramping rate of 2.3 °C/min and holding the synthesis at 265 °C for 1.5 h. For CuIn(S$_{0.65}$Se$_{0.35}$)$_2$ and CuIn$_{0.5}$Ga$_{0.5}$Se$_2$ nanocrystals, the synthetic procedure was the same as CuInSSe synthesis except with different reactant contents: CuIn(S$_{0.65}$Se$_{0.35}$)$_2$, 120 mL of oleylamine, 0.495 g of CuCl, 1.106 g of InCl$_3$, 0.276 g of Se, and 0.209 g of S; CuIn$_{0.5}$Ga$_{0.5}$Se$_2$, 120 mL of oleylamine, 0.495 g of CuCl, 0.553 g of InCl$_3$, 0.440 g of GaCl$_3$, and 0.789 g of Se.

Characterization. The nanocrystals were characterized using various analytical techniques, including transmission electron microscopy (TEM), energy-dispersive X-ray spectroscopy (EDS), X-ray diffraction (XRD), X-ray photoelectron spectroscopy (XPS), and UV−vis−NIR absorbance spectrophotometer.

The TEM samples were prepared by drop-casting the as-prepared nanocrystals in hexane dispersion onto carbon-coated 200 mesh titanium or nickel TEM grids. Hitachi H-7100 TEM and JEOL JEM-1200 were used for low resolution TEM imaging. HRTEM images were acquired on a Tecnai G^2 F20 X-Twin microscope at an accelerating voltage of 200 kV. The HRTEM microscope is equipped with an Oxford INCA EDS detector for EDS data collection. XRD analyses were performed on a Rigaku Ultima IV X-ray diffractometer using a Cu Kα radiation source (λ = 1.54 Å). For XRD sample characterization, the nanocrystals were evaporated from concentrated dispersions onto glass substrates. Diffraction data were collected by scanning for 12 h at a rate of 0.016 deg/s. XPS data were acquired on a Kratos Axis Ultra DLD using a 500 mm Rowland circle Al monochromator. For XPS sample preparation, the nanocrystals were drop-casted on a 0.5 × 0.5 cm wafer in an argon-filled glovebox. UV−vis−NIR absorbance spectra of nanocrystals dispersion in toluene were obtained by a JASCO V-570 UV−vis−NIR spectrophotometer.

■ RESULTS AND DISCUSSION

$CuIn(S_{1-x}Se_x)_2$ nanocrystals were synthesized by a modified heating-up method developed by Panthani et al.[14] and Guo et al.[16] CuCl, InCl$_3$, S, and Se were used as Cu, In, S, and Se precursor sources, respectively. In a typical reaction, a combination of precursors with desired individual mole ratio with oleyamine was placed in a glass flask connected to a Schlenk line system. The flask was heated to 130 °C for degassing, heated to 265 °C with a temperature ramping rate of 2.3 °C/min, and left for several hours to enable nanocrystal growth and stoichiometric alloying. To achieve the formation of $CuIn(S_{1-x}Se_x)_2$ quaternary nanocrystals with controlled S/Se ratio, keeping a temperature ramping profile at a slow and constant rate is the most important key. Oleylamine has multifunctional roles for nanocrystal synthesis. First, CuCl (or InCl$_3$) salts readily dissolved in oleylamine to form a liquid metal [CuCl−oleylamine] (or [InCl$_3$−oleylamine]) complex at room temperature. These complexes exhibit good stability, which might be due to the formation of a N−H···Cl hydrogen bonding.[46] The decomposition of the liquid complex provides sufficient Cu (or In) supply for nanocrystal growth. On the other hand, S and Se powder were not soluble in oleylamine, but they immediately melted above their melting points (Se, 220 °C; S, 120 °C) and mixed homogeneously with reaction solution. Second, as discussed by Pan et al.,[40] oleylamine could reduce the relative reactivity between Cu, In, S, and Se reactants, which is crucial for successful stoichiometry-controlled nanocrystal synthesis. Third, oleylamine can passivate the growing nuclei and decelerate the growth rate of nanocrystals at reactions, so obtained nanocrystals had smaller size and morphology deviation. Finally, oleylamine-capped $CuIn(S_{1-x}Se_x)_2$ nanocrystals could form stable nanocrystal dispersion in a wide range of organic solvents for months, making them ideal nanocrystal inks for further photovoltaic applications.

Synthesis of CuInSSe Nanocrystals. Figure 1 shows the synthesis result by decomposing 0.5 mmol of individual Cu, In, S, and Se reactants in the presence of oleylamine at 265 °C.
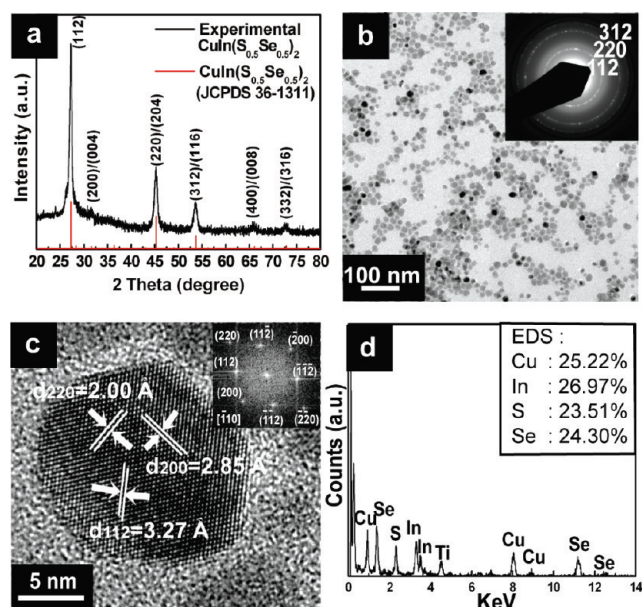
Figure 1. (a) XRD pattern of CuInSSe nanocrystals. The peaks have been indexed to tetragonal chalcopyrite of CuInSSe (JCPDS no. 36-1311). (b) TEM image of CISSe nanocrystals. Inset: Indexed SAED pattern. (c) HRTEM image of a CuInSSe nanocrystal projected in the [$\bar{1}$10] orientation. Inset: The corresponding FFT pattern. (d) Element composition of a field of CuInSSe nanocrystals measured by EDS. The Ti and C signals in the EDS data are from the titanium TEM grid and the carbon support.

The XRD pattern (Figure 1a) from the product shows three major diffraction peaks at 27.28, 45.26, and 53.65, which can be indexed to the (112), (220)/(204), and (312)/(116) of tetragonal chalcopyrite structure of CuInSSe (JCPDS no. 36-1311), respectively. There were no other measurable phases produced in the synthesis. Figure 1b shows TEM images of nanocrystals with size polydispersity, with an average diameter of approximately 16.6 nm and a size deviation of 3.24 nm (Table S1). The selected-area electron diffraction pattern (SAED) of a field of nanoparticles shows three diffraction rings, in agreement with the (112), (220), and (312) of the chalcopyrite phase of CuInSSe, respectively. Figure 1c shows a high-resolution TEM image of a nanocrystal, showing its primarily ordered single-crystal structure, with interplanar d-spacings of 2.00, 2.85, and 3.27 Å corresponding to the (220), (200), and (112) planes of chalcopyrite CuInSSe, respectively. The fast Fourier transforms (FFTs) of the nanocrystal (Figure 1c, inset) are also consistent with chalcopyrite CuInSSe. EDS (Figure 1d) of a field of nanocrystals gave an average Cu/In/S/Se composition of 0.25:0.27:0.24:0.24 matching greatly with the target mole ratio of 0.25:0.25:0.25:0.25. STEM-EDS mapping (Figure 2) of nanocrystals in the selected rectangular area confirmed that Cu, In, S, and Se are equally distributed among the nanocrystals, indicating that CuInSSe nanocrystals are uniformly alloyed. The feature peaks of oleylamine from FTIR analysis show the presence of oleylamine on the nanocrystal surface (Figure S1).

XPS was used to investigate the chemical electronic state of the CuInSSe nanoparticles. All binding energies had been corrected by referencing the C 1s (284.6 eV). Figure 3 shows the XPS spectra of oleylamine-capped CuInSSe nanocrystals. Figure 3a shows the Cu 2p core splitting into Cu 2p$_{3/2}$ (932.1 eV) and Cu 2p$_{1/2}$ (952.0 eV) peaks with a peak separation of 19.9 eV, in
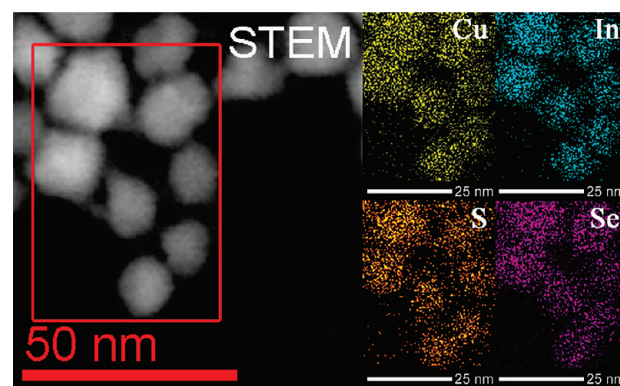

Figure 2. STEM image of CuInSSe nanocrystals. The red rectangular area is the selected area for STEM-EDS elemental mapping of Cu, In, S, and Se, and the individual element mapping result is shown at the right.
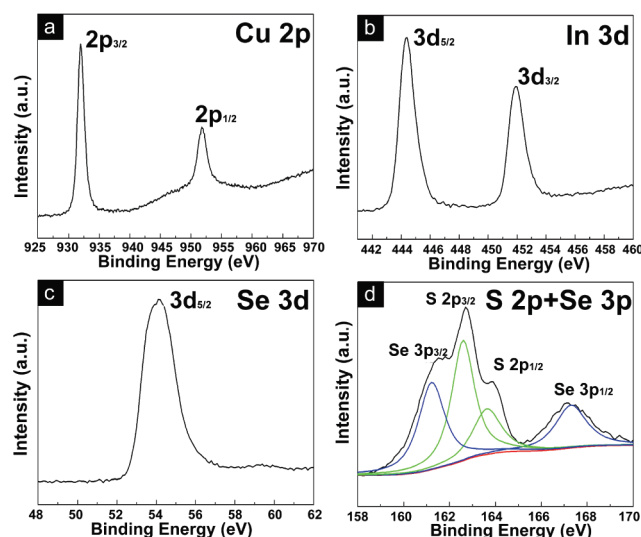

Figure 3. XPS spectrum of the obtained CuInSSe nanocrystals: (a) Cu 2p, (b) In 3d, (c) Se 3d, and (d) S 2p and Se 3p core levels. The green lines are contributed from the S 2p orbital, and the blue lines are contributed from the Se 3p orbital, respectively. The fitting procedure used to separate these contributions is described in the text.

agreement with those reported in the literature for the CuInSe$_2$ nanocrystals,[47] suggesting that the copper valence state in the CuInSSe nanocrystals is +1. In addition, we exclude the presence of +2 valence state because the Cu 2p$_{3/2}$ satellite peak of Cu^{2+} (942 eV) did not appear in the spectrum. Figure 3b shows the In 3d peaks located at 444.4 and 451.9 eV with a peak separation of 7.5 eV, consistent with a valence of +3.[40,47] Figure 3c shows the Se 3d$_{5/2}$ peak located at 54.1 eV, indicating Se^{2-}. Figure 3d shows the S 2p and Se 3p core levels, which were fitted to doublets by a mixed Gaussian and Lorentzian profile. S 2p core splits into S 2p$_{3/2}$ (162.5 eV) and S 2p$_{1/2}$ (163.6 eV) peaks with a peak separation of 1.1 eV.[48] The two peaks of S 2p in Figure 3d were assigned to S 2p binding energy with a valence of −2, which is the characteristic of sulfide (i.e., S bonded to copper or indium). The Se 3p core splits into two peaks of Se 3p$_{3/2}$ (161.1 eV) and Se 3p$_{1/2}$ (167.1 eV) with a peak separation of 6.0 eV. The peak-shift value of Se 3p and the location of binding energy of both S 2p and Se 3p are in good accordance with those values reported.[49]

**Table 1. Composition, Lattice Parameters (a and c), and Optical Band Gap Energies of $CuIn(S_{1-x}Se_x)_2$ Nanocrystals**

target compound $CuIn(S_{1-x}Se_x)_2$	precursor composition (Cu/In/S/Se atom ratio %)	composition measured by EDS[a] (Cu/In/S/Se atom ratio %)	a (Å)[b]	c (Å)[b]	E_g (eV)[c]
$CuInS_2$ ($x = 0$)	25:25:50:0 (1:1:2:0)	24.39:25.76:49.85:0 (0.98:1.03:1.99:0)	5.52	11.02	1.46
$CuIn(S_{0.85}Se_{0.15})_2$ ($x = 0.15$)	25:25:42.5:7.5 (1:1:1.7:03)	23.71:26.46:43.72:6.11 (0.95:1.06:1.75:0.24)	5.57	11.10	1.35
$CuIn(S_{0.65}Se_{0.35})_2$ ($x = 0.35$)	25:25:32.5:17.5 (1:1:1.3:0.7)	27.39:24.23:30.14:18.24 (1.09:0.97:1.21:0.73)	5.62	11.21	1.25
$CuIn(S_{0.5}Se_{0.5})_2$ ($x = 0.5$)	25:25:25:25 (1:1:1:1)	25.22:26.97:23.51:24.30 (1.01:1.08:0.94:0.97)	5.67	11.32	1.18
$CuIn(S_{0.35}Se_{0.65})_2$ ($x = 0.65$)	25:25:17.5:32.5 (1:1:0.7:1.3)	23.12:25.25:18.59:33.04 (0.93:1.01:0.74:1.32)	5.71	11.40	1.11
$CuIn(S_{0.15}Se_{0.85})_2$ ($x = 0.85$)	25:25:7.5:42.5 (1:1:0.3:1.7)	23.93:25.74:6.77:43.56 (0.96:1.03:0.27:1.74)	5.76	11.52	1.05
$CuInSe_2$ ($x = 1$)	25:25:0:50 (1:1:0:2)	23.83:24.23:0:51.94 (0.95:0.97:0:2.08)	5.79	11.62	0.98

[a] EDS measurements have an error of ca. ±2 atom %. [b] Lattice parameters (a and c) were determined from XRD patterns. [c] Optical band gap energies (E_g) were determined from UV−vis−NIR spectra.
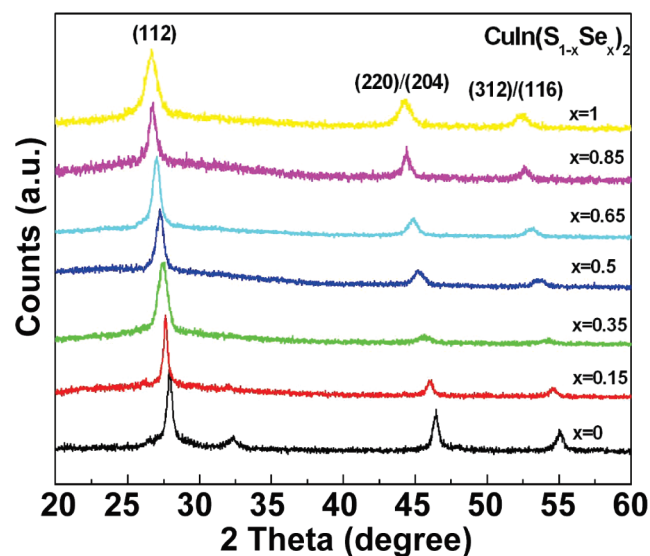
Figure 4. (a) XRD patterns of $CuIn(S_{1-x}Se_x)_2$ nanocrystals prepared at 265 °C.

Synthesis of $CuIn(S_{1-x}Se_x)_2$ Nanocrystals. The S/Se composition ratio in $CuIn(S_{1-x}Se_x)_2$ nanocrystals could be tuned across the entire x range from 0 to 1 by varying the S/Se reactant ratio. Figure 4 shows XRD data of $CuIn(S_{1-x}Se_x)_2$ nanocrystals synthesized in the reactions of S/Se reactant ratio varying from 0 to 1. The variation between the S/Se ratio in the $CuIn(S_{1-x}Se_x)_2$ nanoparticles is clearly reflected from XRD data. At $x = 0$, the XRD data correspond to those of chalcopyrite $CuInS_2$ (JCPDS no. 27-0159). As the Se content increases, the diffraction peaks gradually shift toward lower 2θ angle, which is attributed to the increased lattice spacings of larger Se atoms (1.98 Å) substitution for smaller S atoms (1.84 Å). At $x = 1$, the XRD data could be indexed to chalcopyrite $CuInSe_2$ (JCPDS no. 40-1487). The lattice parameters (a and c) of tetragonal $CuIn(S_{1-x}Se_x)_2$ nanocrystals determined from XRD patterns are listed in Table 1. Figure 5 shows the plot of $CuIn(S_{1-x}Se_x)_2$ lattice parameters as a function of x. Our fitting has shown that the lattice parameters have a linear relation with Se composition, which is in agreement with Vegard's law.

Figure 6 shows TEM images of $CuIn(S_{1-x}Se_x)_2$ with x ranging from 0 to 1. The sizes of $CuIn(S_{1-x}Se_x)_2$ nanocrystals range from 14.9 to 16.6 nm, and the statistical analysis of particle size is shown in Table S1. The variation of the average sizes of $CuIn(S_{1-x}Se_x)_2$ nanocrystals gives a standard deviation of
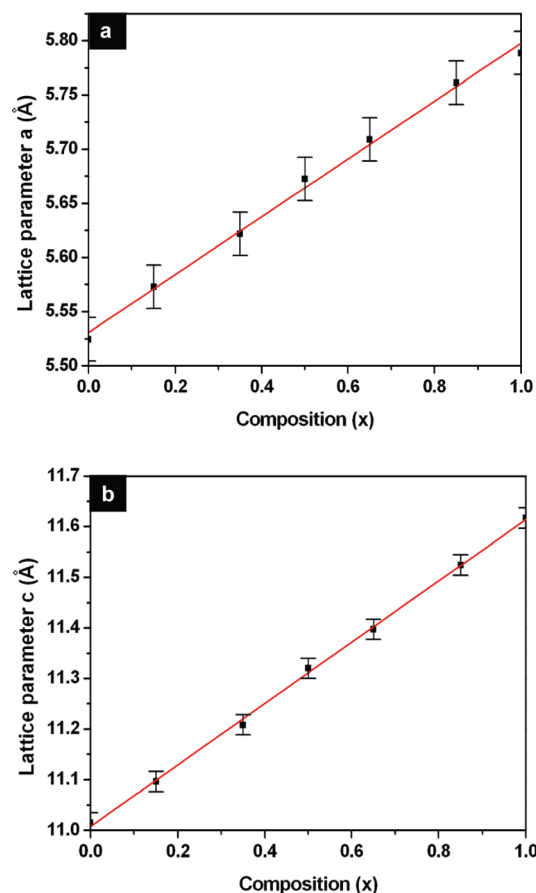
Figure 5. Relationship between the change of (a) lattice parameter a and (b) lattice parameter c with x of $CuIn(S_{1-x}Se_x)_2$ nanocrystals. The error bars are the statistical fluctuations of each different, randomly selected sample.

15−30% of mean value. Figure 7 shows the HRTEM images of each different composition $CuIn(S_{1-x}Se_x)_2$ nanocrystal with clear imaged lattice fringes. As the Se content increases, the lattice spacings of $d_{(112)}$ in each nanocrystal increase gradually, which are in agreement with the change trend of d-spacing values of (112) plane obtained from powder XRD patterns. The chemical compositions of $CuIn(S_{1-x}Se_x)_2$ nanocrystals were analyzed by EDS as shown in Figure 8. Quantitative elemental EDS analyses of these nanocrystals are listed in Table 1. EDS spectra of nanocrystals indicate the presence of Cu, In, S,
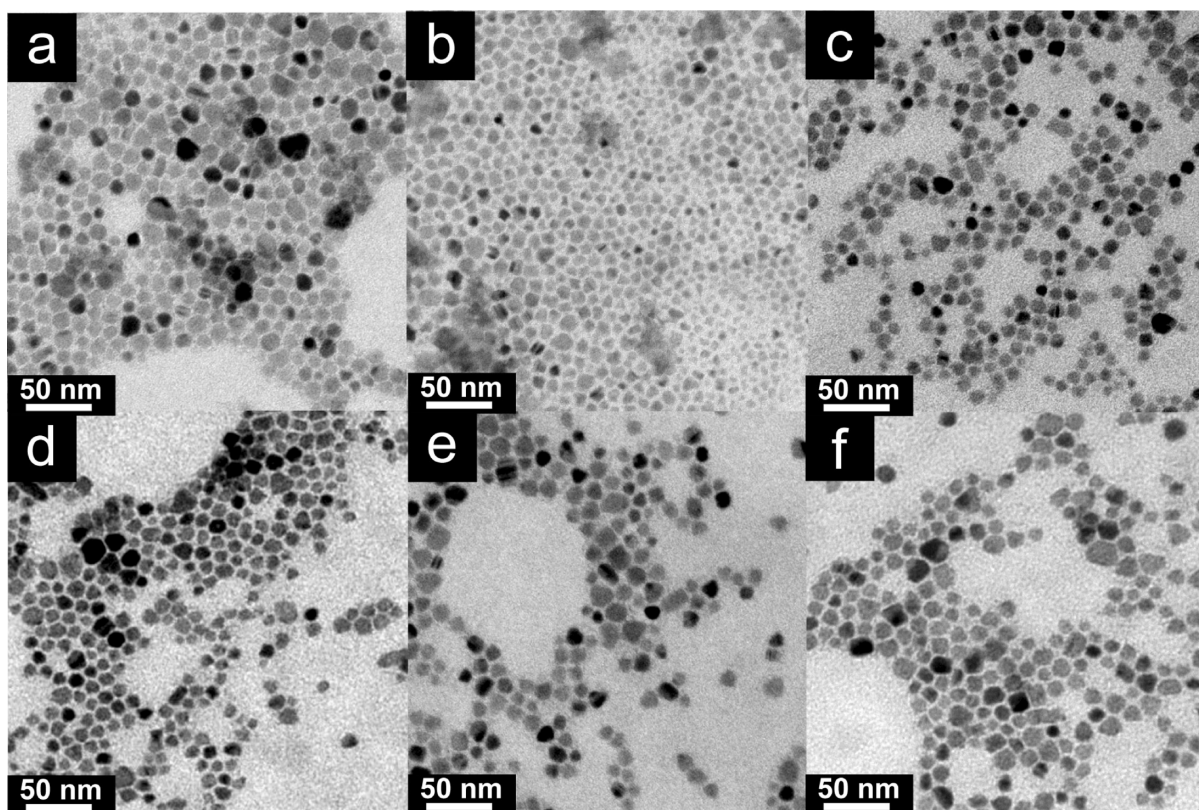
1595

dx.doi.org/10.1021/jp1090735 |*J. Phys. Chem. C* 2011, 115, 1592–1599

Figure 6. TEM images of $CuIn(S_{1-x}Se_x)_2$ nanocrystals with (a) $x = 0$, (b) $x = 0.15$, (c) $x = 0.35$, (d) $x = 0.65$, (e) $x = 0.85$, and (f) $x = 1$.

Figure 7. HRTEM images of $CuIn(S_{1-x}Se_x)_2$ nanocrystals with (a) $x = 0$, (b) $x = 0.15$, (c) $x = 0.35$, (d) $x = 0.65$, (e) $x = 0.85$, and (f) $x = 1$. The nanocrystals were all imaged down the $[\bar{1}10]$ crystallographic zone axis.
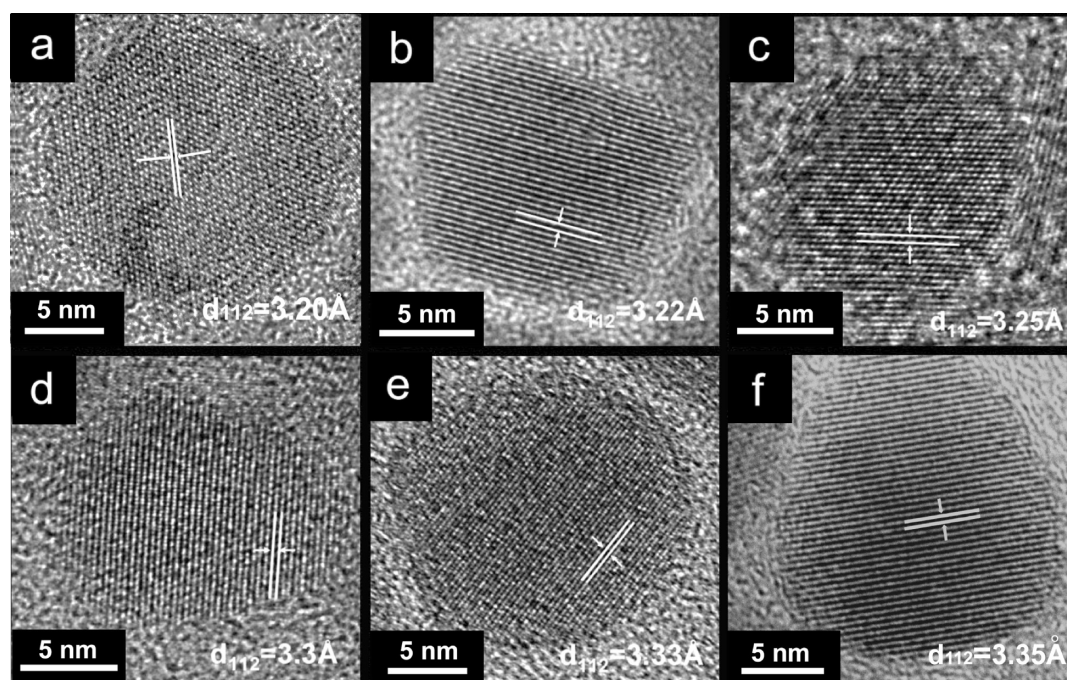
and Se. The peak intensity of Se gradually increases with increasing the Se content, whereas the intensity of S decreases. The relationship between the Se content of precursors and those obtained from EDS of nanocrystals gave a linear trend (Figure 8b). The Cu:In:S:Se mole ratios of $CuIn(S_{1-x}Se_x)_2$ nanocrystals measured from EDS are close to those calculated on the basis of the precursors used, as summarized in Table 1.
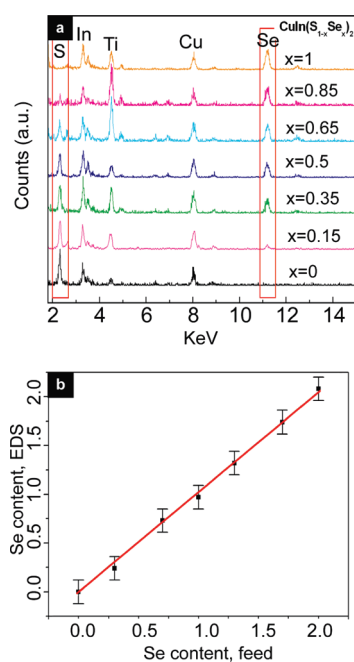
Figure 8. (a) TEM-EDS spectra of $CuIn(S_{1-x}Se_x)_2$ nanocrystals. (b) Relationship between the Se contents in the feed versus those in the product as determined by EDS. The error bars represent the uncertainty of the instrument measurements.

Figure 9 shows UV−vis−NIR absorption spectra of a series of optically clear $CuIn(S_{1-x}Se_x)_2$ nanocrystal solutions. The band-edge absorption of the $CuIn(S_{1-x}Se_x)_2$ nanocrystals exhibited a gradual red shift toward longer wavelength while increasing Se composition, which is due to a narrower band gap of $CuInSe_2$ (0.98 eV) than that of $CuInS_2$ (1.46 eV). The optical band gaps of nanocrystals were calculated by extrapolation of the α^2-$h\nu$ line to the horizontal axis and are listed in Table 1. To further understand the relation between the alloy composition and their band gap evolution, Figure 9b shows the plot of the band gap of nanocrystals as a function of x. It was found that the optical band gap of samples shows a curve, which is termed as band gap "bowing".[50] The data points were fitted by the modified bowing equation as follows:

$$E_g(x) = xE_g^{CuInSe_2} + (1-x)E_g^{CuInS_2} - x(1-x)b$$

where $E_g^{CuInSe2}$ and E_g^{CuInS2} are band gap energies of $CuInSe_2$ and $CuInS_2$, respectively; b is the bowing parameter describing the nonlinear relationship between band gap and composition. The bowing parameter of $CuIn(S_{1-x}Se_x)_2$ nanocrystals determined by this equation is 0.17 eV, which slightly deviates from the linear relation and shows a nonlinear dependence of band gap and x in $CuIn(S_{1-x}Se_x)_2$ nanocrystals. However, the derived bowing parameter (0.17 eV) was consistent with reported values of bulk $CuIn(S_{1-x}Se_x)_2$.[18,20] This nonlinear relation could possibly arise from three sources: (i) the change of band structure due to lattice constant variation, (ii) electron distribution deformation due to the alloy atoms' electronegativity differences, and (iii) relaxation of anion−cation bond lengths and angles.[51,52]

Gram-Scale Production of $CuIn(S_{1-x}Se_x)_2$ and $CuIn_{1-x}Ga_xSe_2$ Nanocrystals. Under well-controlled reaction chemistry,

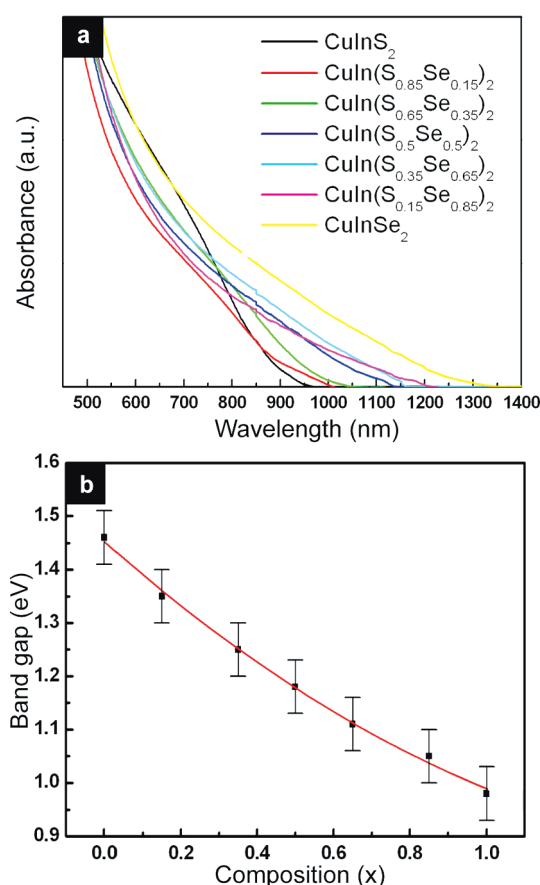**Figure 9.** (a) UV−vis−NIR absorption spectra of the $CuIn(S_{1-x}Se_x)_2$ nanocrystals dispersed in toluene. (b) Plot of the optical band gaps versus with composition x. The error bars are the uncertainties in the determination of the optical band gap of nanocrystals.

a heating-up method poses advantageous features for large-scale production of nanocrystals because the synthesis can be carried out as a reaction with a high concentration of reactants in a large-volume reactor.[53] Figure 10 shows the result of CuInSSe nanocrystal synthesis by decomposition of 5 mmol of individual Cu, In, S, and Se reactants in the presence of 120 mL of oleylamine in a 500 mL flask at 265 °C. Figure 10a−c shows the obtained 1.08 g of dried CuInSSe nanocrystals powders exhibiting a dark black color due to their red-edge optical absorption (see Figure S2 for the weighing photographs). CuInSSe nanocrystals obtained from the scale-up synthesis remain high quality as indicated in TEM imaging and with good stoichiometric control as confirmed by XRD and UV−vis− NIR absorption spectra, respectively. Figure 10d show 1.18 g of $CuIn(S_{0.65}Se_{0.35})_2$ nanocrystals obtained in a scale-up reaction and their corresponding TEM, XRD, and UV−vis−NIR data (Figure 10e,f). In addition to $CuIn(S_{1-x}Se_x)_2$ nanocrystals, we also extend the scale-up synthesis for gram-scale production of stoichiometry-controlled $CuIn_{1-x}Ga_xSe_2$ nanocrystals. As shown in Figure 10g−i, 1.25 g of $CuIn_{0.5}Ga_{0.5}Se_2$ nanocrystals with controlled stoichiometry could be obtained.[14] These results indicate that the developed heating-up in this study could be utilized as a general method to produce large quantities of stoichiometry-controlled quaternary I−III−VI$_2$ compound nanocrystals. These nanocrystals are potential materials used for CIS or CIGS absorber film fabrication, but property comparison between nanocrystals and films made of these nanocrystals requires further study.
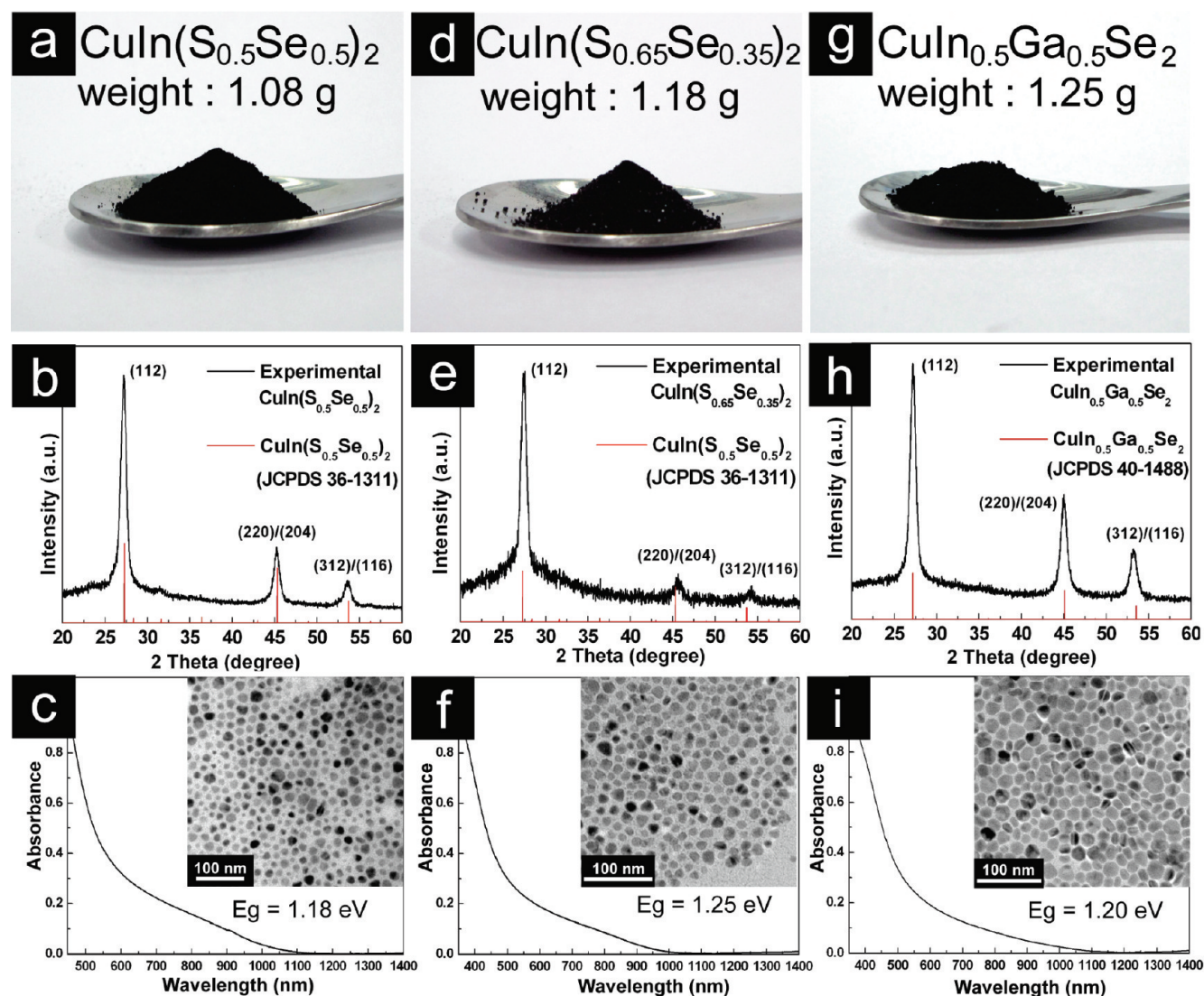
Figure 10. Gram-scale production of (a−c) CuInSSe, (d−f) $CuIn(S_{0.65}Se_{0.35})_2$, and (g−i) $CuIn_{0.5}Ga_{0.5}Se_2$ nanocrystals.

CONCLUSIONS

High-quality, high-yield of chalcopyrite quaternary $CuIn(S_{1-x}Se_x)_2$ ($0 \leq x \leq 1$) nanocrystals with composition tunable across the entire $x = 0-1$ range have been synthesized. The lattice parameters (a and c) of nanocrystals increased linearly with respect to x, following Vegard's law. The band gap energies of $CuIn(S_{1-x}Se_x)_2$ nanocrystals could be tuned from 0.98 to 1.46 eV by decreasing the Se content, yielding a nonlinear relation with x having a bowing constant of 0.17 eV, in agreement with its bulk values. These high-quality nanocrystals can be dispersed in most organic solvents and could be readily used in the form of nanocrystal inks for the preparation of CIS absorber. Gram quantities of stoichiometry-controlled $CuIn(S_{1-x}Se_x)_2$ and $CuIn_{1-x}Ga_xSe_2$ nanocrystals could be also obtained by the method developed in this study, demonstrating its potential for providing ultralarge quantities (e.g., kilograms) of stoichiometry-tunable I−III−VI$_2$ compound nanocrystals in applications for low-cost non-vacuum-based CIGS solar cells.

ASSOCIATED CONTENT

S **Supporting Information.** Statistical size distribution and FTIR of CuInSSe nanocrystals and weighting photographs of gram-scale synthesis product. This material is available free of charge via the Internet at http://pubs.acs.org.

AUTHOR INFORMATION

Corresponding Author
*Tel.: + 886-3-572-3661. Fax: + 886-3-571-5408. E-mail: hytuan@che.nthu.edu.tw.

Author Contributions
†These authors contributed equally.

■ REFERENCES

(1) Guillemoles, J.; Rau, U.; Kronik, L.; Schock, H.; Cahen, D. *Adv. Mater.* **1999,** *11*, 957.

(2) Stanbery, B. J. *Crit. Rev. Solid State Mater. Sci.* **2002,** *27*, 73.

(3) Ramanathan, K.; Contreras, M. A.; Perkins, C. L.; Asher, S.; Hasoon, F. S.; Keane, J.; Young, D.; Romero, M.; Metzger, W.; Noufi, R.; Ward, J.; Duda, A. *Prog. Photovoltaics Res. Appl.* **2003,** *11*, 225.

(4) Stolt, L.; Hedstrom, J.; Kessler, J.; Ruckh, M.; Velthaus, K. O.; Schock, H. W. *Appl. Phys. Lett.* **1993,** *62*, 597.

(5) AbuShama, J.; Johnston, S.; Moriarty, T.; Teeter, G.; Ramanathan, K.; Noufi, R. *Prog. Photovoltaics Res. Appl.* **2004,** *12*, 39.

(6) Hibberd, C. J.; Chassaing, E.; Liu, W.; Mitzi, D. B.; Lincot, D.; Tiwari, A. N. *Prog. Photovoltaics Res. Appl.* **2010,** *18*, 434.

(7) Hillhouse, H. W.; Beard, M. C. *Curr. Opin. Colloid Interface Sci.* **2009,** *14*, 245.

(8) Li, L.; Coates, N.; Moses, D. *J. Am. Chem. Soc.* **2010,** *132*, 22.

(9) Norako, M. E.; Brutchey, R. L. *Chem. Mater.* **2010,** *22*, 1613.

(10) Wooten, A. J.; Werder, D. J.; Williams, D. J.; Casson, J. L.; Hollingsworth, J. A. *J. Am. Chem. Soc.* **2009,** *131*, 16177.

(11) Norako, M. E.; Franzman, M. A.; Brutchey, R. L. *Chem. Mater.* **2009,** *21*, 4299.

(12) Batabyal, S. K.; Tian, L.; Venkatram, N.; Ji, W.; Vittal, J. J. *J. Phys. Chem. C* **2009,** *113*, 15037.

(13) Koo, B.; Patel, R. N.; Korgel, B. A. *J. Am. Chem. Soc.* **2009,** *131*, 3134.

(14) Panthani, M. G.; Akhavan, V.; Goodfellow, B.; Schmidtke, J. P.; Dunn, L.; Dodabalapur, A.; Barbara, P. F.; Korgel, B. A. *J. Am. Chem. Soc.* **2008,** *130*, 16770.

(15) Guo, Q.; Kim, S. J.; Kar, M.; Shafarman, W. N.; Birkmire, R. W.; Stach, E. A.; Agrawal, R.; Hillhouse, H. W. *Nano Lett.* **2008,** *8*, 2982.

(16) Guo, Q.; Ford, G. M.; Hillhouse, H. W.; Agrawal, R. *Nano Lett.* **2009,** *9*, 3060.

(17) Pan, D. C.; An, L. J.; Sun, Z. M.; Hou, W.; Yang, Y.; Yang, Z. Z.; Lu, Y. F. *J. Am. Chem. Soc.* **2008,** *130*, 5620.

(18) Mudryi, A. V.; Victorov, I. A.; Gremenok, V. F.; Patuk, A. I.; Shakin, I. A.; Yakushev, M. V. *Thin Solid Films* **2003,** *431−432*, 197.

(19) Bekker, J. *Sol. Energy Mater. Sol. Cells* **2009,** *93*, 539.

(20) Neff, H.; Lange, P.; Fearheiley, M. L.; Bachman, K. J. *Appl. Phys. Lett.* **1985,** *47*, 1089.

(21) Landry, C. C.; Lockwood, J.; Barron, A. R. *Chem. Mater.* **1995,** *7*, 699.

(22) Landry, C. C.; Barron, A. R. *Science* **1993,** *260*, 1653.

(23) Zeaiter, K.; Llinares, Y.; Llinares, C. *Sol. Energy Mater. Sol. Cells* **2000,** *61*, 313.

(24) Shirakata, S.; Terasako, T.; Kariya, T. *J. Phys. Chem. Solids* **2005,** *66*, 1970.

(25) Alberts, V.; Dejene, F. D. *J. Phys. D: Appl. Phys.* **2002,** *35*, 2021.

(26) Yamamoto, Y.; Yamaguchi, T.; Demizu, Y.; Tanaka, T.; Yoshida, A. *Thin Solid Films* **1996,** *282*, 372.

(27) Liu, W.; Mitzi, D. B.; Yuan, M.; Kellock, A. J.; Chey, S. J.; Gunawan, O. *Chem. Mater.* **2010,** *22*, 1010.

(28) Hou, W. W.; Bob, B.; Li, S. H.; Yang, Y. *Thin Solid Films* **2009,** *517*, 6853.

(29) Xiao, J.; Xie, Y.; Xiong, Y.; Tang, R.; Qian, Y. *J. Mater. Chem.* **2001,** *11*, 1417.

(30) Alivisatos, A. P. *Science* **1996,** *271*, 933.

(31) Regulacio, M. D.; Han, M. Y. *Acc. Chem. Res.* **2010,** *43*, 621.

(32) Zhong, X. H.; Han, M. Y.; Dong, Z. L.; White, T. J.; Knoll, W. *J. Am. Chem. Soc.* **2003,** *125*, 8589.

(33) Zhong, X. H.; Feng, Y. Y.; Knoll, W.; Han, M. Y. *J. Am. Chem. Soc.* **2003,** *125*, 13559.

(34) Swafford, L. A.; Weigand, L. A.; Bowers, M. J.; McBride, J. R.; Rapaport, J. L.; Watt, T. L.; Dixit, S. K.; Feldman, L. C.; Rosenthal, S. *J. Am. Chem. Soc.* **2006,** *128*, 12299.

(35) Bailey, R. E.; Nie, S. M. *J. Am. Chem. Soc.* **2003,** *125*, 7100.

(36) Arachchige, I. U.; Kanatzidis, M. G. *Nano Lett.* **2009,** *9*, 1583.

(37) Shieh, F.; Sunders, A. E.; Korgel, B. A. *J. Phys. Chem. B* **2005,** *109*, 8538.

(38) Camargo, P. H. C.; Lee, Y. H.; Jeong, U.; Zou, Z. Q.; Xia, Y. N. *Langmuir* **2007,** *23*, 2985.

(39) Tang, J.; Hinds, S.; Kelley, S. O.; Sargent, E. H. *Chem. Mater.* **2008,** *20*, 6906.

(40) Pan, D. C.; Wang, X. L.; Zhou, Z. H.; Chen, W.; Xu, C. L.; Lu, Y. F. *Chem. Mater.* **2009,** *21*, 2489.

(41) Sunc, C.; Gardner, J. S.; Long, G.; Bajracharya, C.; Thurber, A.; Punnoose, A.; Rodriguez, R. G.; Pak, J. J. *Chem. Mater.* **2010,** *22*, 2699.

(42) Torimoto, T.; Adachi, T.; Okazaki, K.-I.; Sakuraoka, M.; Shibayama, T.; Ohtani, B.; Kudo, A.; Kuwabata, S. *J. Am. Chem. Soc.* **2007,** *129*, 12388.

(43) Pan, D. C.; Weng, D.; Wang, X. L.; Xiao, Q. F.; Chen, W.; Xu, C. L.; Yang, Z. Z.; Lu, Y. F. *Chem. Commun.* **2009,** *28*, 4221.

(44) Deng, Z.; Yan, H.; Liu, Y. *J. Am. Chem. Soc.* **2009,** *131*, 17744.

(45) Dai, P.; Shen, X.; Lin, Z.; Feng, Z.; Xu, H.; Zhan, J. *Chem. Commun.* **2010,** *46*, 5749.

(46) Jones, P. G.; Ahrens, B. *New J. Chem.* **1998,** *22*, 1041.

(47) Wang, J. J.; Wang, Y. Q.; Cao, F. F.; Guo, Y. G.; Wan, L. J. *J. Am. Chem. Soc.* **2010,** *132*, 12218.

(48) Zhong, H. Z.; Zhou, Y.; Ye, M. F.; He, Y. J.; Ye, J. P.; He, C.; Yang, C. H.; Li, Y. F. *Chem. Mater.* **2008,** *20*, 6434.

(49) Sporken, R.; Abuel-Rub, K. M.; Chen, Y. P.; Sivananthan, S. *J. Electron. Mater.* **1998,** *27*, 776.

(50) Razeghi, M. *Fundamentals of Solid State Engineering*, 2nd ed.; Springer-Verlag: New York, 2005.

(51) Bernard, J. E.; Zunger, A. *Phys. Rev. B* **1987,** *36*, 3199.

(52) Wei, S. H.; Zhang, S. B.; Zunger, A. *J. Appl. Phys.* **2000,** *87*, 1304.

(53) Park, J.; An, K. J.; Hwang, Y. S.; Park, J. G.; Noh, H. J.; Kim, J. Y.; Park, J. H.; Hwang, N. M.; Hyeon, T. *Nat. Mater.* **2004,** *3*, 891.